RF ELECTRON GUNS WITH CONTROLLED LONGITUDINAL DISPERSION FOR ATTOSECOND UED*

Y. Cheng, Shanghai Institute of Applied Physics, Pudong, China
Ch. Feng, Q. gu†, Shanghai Advanced Research Institute, Pudong, China

Abstract

We formulate the design of a UED-oriented RF gun as a constrained longitudinal-dynamics problem and obtain a nonuniform 2.33-cell S-band solution with controlled longitudinal dispersion. The representative solution, $(0.4, 0.93, 1)$, operated near 45 MV/m, brings the phases of maximum energy gain and minimum time of flight (TOF) into near coincidence and thereby yields a well-defined gun dispersion. For the GPT tracking reported here, the beam at the gun exit has a kinetic energy of 3 MeV, an rms bunch length of 100 fs, a charge of 0.1 pC, and a normalized emittance of about 10 nm · rad. With a matched Double Bend Achromat (DBA) beamline, the bunch is compressed to 940 as rms with 10 fC charge at the sample. For RF-amplitude, RF-phase, charge, and magnet-field jitters of 0.05%, 0.2 ps, 3%, and 0.01% rms, respectively, the sample-plane arrival-time jitter is 600 as rms; source-only scans give 518 as rms from amplitude jitter and 167 as rms from phase jitter. These results show that the proposed model provides a direct route to RF guns specifically suited for attosecond UED.

INTRODUCTION

The temporal resolution of MeV ultrafast electron diffraction (UED) is limited jointly by the bunch duration and the shot-to-shot arrival-time jitter [1]. In present MeV UED beamlines, the RF gun remains one of the dominant sources of timing noise. The widely used 1.6-cell photoinjector was originally developed for FEL injectors and is highly effective for producing low projected energy spread, but its exit momentum and time of flight are not cleanly correlated [2]. As a result, RF phase and amplitude fluctuations are readily transferred into timing jitter. Downstream isochronous transport can compensate part of the momentum-dependent timing variation [3, 4], but a design principle for an RF gun specifically aimed at UED has remained lacking.

This work addresses that gap. We formulate the design of a UED-oriented RF gun as a constrained longitudinal-dynamics problem. The target is not minimum energy spread alone; rather, the gun is required to operate near a phase at which maximum energy gain and minimum TOF nearly coincide, so that the gun exit acquires a clean momentum–TOF correlation and admits a characteristic dispersion R^g_{56}. The model naturally yields a nonuniform 2.33-cell solution. We then analyze its longitudinal response, compare it directly with the conventional 1.6-cell gun, and verify with a DBA beamline that the resulting source supports attosecond-level compression and sub-femtosecond timing stability at the sample.

THEORETICAL MODEL

We formulate the RF-gun design as a constrained longitudinal-dynamics problem. For an N-cell gun, the cell lengths are written as

$$L_i = \alpha_i \frac{\lambda}{2}, \qquad L(\alpha) = \sum_{i=1}^{N} L_i, \tag{1}$$

where α_i is the dimensionless cell-length parameter and $\lambda = c/f$ is the RF wavelength. Let E_0 denote the peak accelerating field and ϕ_0 the launch phase at the cathode. With $\psi(z) = \omega t - kz + \phi_0$, the longitudinal dynamics is governed by

$$\frac{d\gamma}{dz} = \frac{eE_0}{mc^2} u(z;\alpha) \sin\psi, \qquad \frac{d\psi}{dz} = k\left(\frac{1}{\beta} - 1\right), \qquad \frac{dt}{dz} = \frac{1}{c\beta}, \tag{2}$$

which define the exit kinetic energy $W(\alpha, E_0, \phi_0) = mc^2[\gamma(L) - 1]$ and the time of flight $T(\alpha, E_0, \phi_0) = t(L)$. The design condition is imposed at a common operating phase ϕ^* by

$$W(\alpha, E_0, \phi^*) = W^*, \quad \partial_\phi W(\alpha, E_0, \phi^*) = 0, \quad \partial_\phi T(\alpha, E_0, \phi^*) = 0. \tag{3}$$

For the present design we consider a three-cell structure, $\alpha = (\alpha_1, \alpha_2, \alpha_3)$. Three cells are sufficient to separate the three physical roles required here: the first cell controls the early nonrelativistic phase slippage, the second cell adjusts the transition into the high-energy regime, and the third cell provides the final near-relativistic energy gain. The first cell is shortened because the beam is still far from relativistic immediately after emission, so the phase advance accumulated there has the largest leverage on the relative location of the maximum-energy and minimum-TOF phases. The second cell is retained close to a full cell and only weakly tuned, because its role is to compensate the phase-slip change introduced by the shortened first cell while preserving efficient acceleration and field balance. The third cell is fixed as a standard full cell, $\alpha_3 = 1$, since by that stage the beam is already near relativistic and the cell contributes mainly stable energy gain, with little further leverage on phase alignment.

With α_3 fixed, the problem remains underdetermined because the unknowns still include $(\alpha_1, \alpha_2, E_0, \phi^*)$. We therefore introduce the closure functional

$$J(\alpha_1, \alpha_2, E_0) = E_0^2 + \mu(\alpha_2 - 1)^2, \qquad \mu > 0, \tag{4}$$

* also at University of Chinese Academy of Sciences, Beijing, China
† guq@sari.ac.cn

which favors lower operating field and a second cell remaining close to a standard full cell. For the target exit energy $W^* = 3\,\mathrm{MeV}$, the representative solution is $(\alpha_1, \alpha_2, \alpha_3) \approx (0.4, 0.93, 1)$ with $E_0 \approx 45\,\mathrm{MV/m}$, and the operating phase is located in the high-phase region near 65°. This solution is not an arbitrary geometric choice; it is the compact configuration in which low-energy phase slippage, high-energy gain, and TOF stationarity become simultaneously compatible.

Following the one-dimensional approximate treatment of Kim [5], we further retain the reduced phase-slippage description associated with the shortened first cell. Defining

$$u_1(\phi_0) = \frac{eE_0L_1}{mc^2}\sin\phi_0, \qquad t_1 = \frac{L_1}{u_1 c}\sqrt{u_1(2+u_1)}, \quad (5)$$

and

$$\Psi_1(\phi_0) = kL_1\frac{\sqrt{u_1(2+u_1)}}{u_1}, \quad (6)$$

where Ψ_1 denotes the phase advance accumulated across the shortened first cell, the high-energy operating phase is obtained from

$$(\Psi_1 - \phi_a^*)\sin\phi_a^* \simeq \frac{mc^2k}{eE_0}. \quad (7)$$

For $f = 2.856\,\mathrm{GHz}$, $E_0 \approx 45\,\mathrm{MV/m}$, and $(\alpha_1, \alpha_2, \alpha_3) \approx (0.4, 0.93, 1)$, Eq. (7) yields the high-energy branch $\phi_a^* \approx 65°$, consistent with the operating phase obtained from the global constrained formulation.

At the same level of approximation, the whole-gun energy is estimated by

$$K_a \simeq \eta_{\mathrm{gun}}\, eE_0L_{\mathrm{tot}}\sin\phi_a^*, \qquad L_{\mathrm{tot}} = L_1 + L_2 + L_3. \quad (8)$$

Here η_{gun} is the transit-time/envelope factor of the standing-wave field, not a fitted normalization. In a simplified TM_{010}-envelope model, a synchronous particle samples the axial field as $|\cos(\pi z/L_{\mathrm{tot}})|$ rather than as a flat field, so

$$\eta_{\mathrm{gun}} \simeq \left\langle\left|\cos\frac{\pi z}{L_{\mathrm{tot}}}\right|\right\rangle = \frac{1}{\pi}\int_0^{\pi}|\cos\theta|\,d\theta = \frac{2}{\pi}.$$

Thus $K_a \simeq (2/\pi)eE_0L_{\mathrm{tot}}\sin\phi_a^*$. For $E_0 \approx 45\,\mathrm{MV/m}$, $L_{\mathrm{tot}} \approx 0.1223\,\mathrm{m}$, and $\phi_a^* \approx 63°$, this gives $K_a \approx 3.1\,\mathrm{MeV}$, close to the field-map/GPT value of about 3 MeV; finite-cell balance, fringe fields, and nonrelativistic phase slippage account for the residual difference.

LONGITUDINAL DISPERSION OF THE 2.33-CELL RF GUN

The representative solution obtained from the theoretical model is a nonuniform 2.33-cell S-band RF gun with $(\alpha_1, \alpha_2, \alpha_3) \approx (0.4, 0.93, 1)$, operated near $E_0 \approx 45\,\mathrm{MV/m}$. All particle-tracking simulations in this work were performed with the General Particle Tracer (GPT) [6] code. The defining longitudinal property of this gun is the near coincidence of the phases for maximum energy gain and minimum time of flight (TOF).

Figure 1 shows the on-axis field profile together with the phase dependence of the gun-exit beam properties. The shortened first cell shifts the phase slippage while the beam is still nonrelativistic, where the TOF is most sensitive to the launch phase. The second cell, kept close to a full cell, compensates the resulting phase displacement and restores efficient acceleration without undoing the phase alignment established upstream. The third cell remains a standard full cell because, once the beam is near relativistic, its main role is to provide stable final energy gain rather than further reshape the phase-slip dynamics. As a result, the phase of maximum gun-exit energy is driven toward the phase of minimum TOF. For the present gun, both occur in the high-phase region around 63°, where the beam exits the gun at about 3 MeV. This near coincidence is the central longitudinal feature of the 2.33-cell gun: the beam is accelerated at the phase where the gun TOF is simultaneously extremized, so energy and timing cease to vary independently near the operating point.

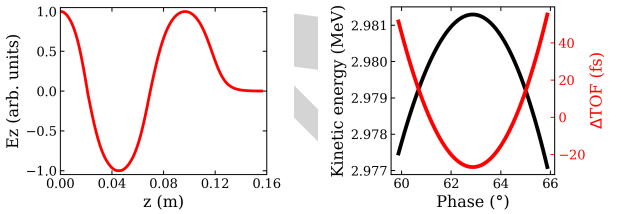

Figure 1: Longitudinal response of the nonuniform 2.33-cell RF gun: (a) on-axis accelerating field, and (b) phase dependence of gun-exit energy and TOF. The maximum-energy and minimum-TOF phases coincide near 63° and 3 MeV.

Figure 2 compares the gun-exit timing response of a conventional 1.6-cell gun and the present 2.33-cell gun under RF phase jitter of ± 0.2 ps and RF-amplitude jitter of $\pm 10^{-3}$. In the 1.6-cell gun, the phase of maximum energy and that of minimum TOF are separated, so the gun-exit TOF and momentum do not form a unique correlation. The blue circles represent amplitude perturbations at fixed RF phase: for a given launch phase, increasing the RF amplitude changes both the beam momentum and the TOF, yielding an amplitude-defined local slope. The red squares represent phase perturbations at fixed RF amplitude: the beam energy changes only weakly, whereas the TOF varies substantially. Under simultaneous amplitude and phase perturbations, the cloud therefore spreads in two partially independent directions, showing that the 1.6-cell gun does not admit a cleanly defined gun dispersion.

In the 2.33-cell gun, by contrast, the near overlap of the maximum-energy and minimum-TOF phases collapses the gun-exit response onto an almost one-to-one energy–TOF curve. Both amplitude and phase perturbations are funneled onto the same longitudinal correlation, so the gun can be characterized by an effective longitudinal dispersion,

$$\Delta t_g \simeq \frac{R_{56}^g}{c}\,\delta, \qquad \delta = \frac{\Delta p}{p}, \quad (9)$$

with $R_{56}^{g} \approx -2.1$ cm. In this regime the first-order sensitivity to RF phase fluctuations is strongly reduced, whereas the residual timing variation remains predominantly amplitude driven and directly correlated with beam momentum.

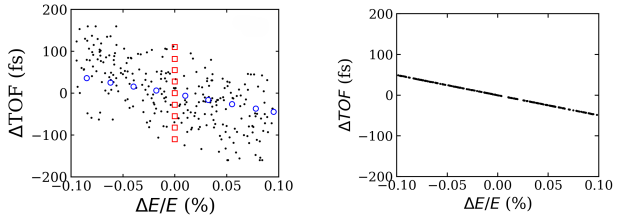

Figure 2: Gun-exit TOF versus relative energy deviation under RF phase jitter of ± 0.2 ps and RF-amplitude jitter of $\pm 10^{-3}$. The 1.6-cell gun gives separated phase and amplitude responses, whereas the 2.33-cell gun collapses them onto an almost one-to-one curve, defining an effective R_{56}^{g}.

SIMULATION RESULTS

Following the DBA concept of Ref. [7], the downstream transport is matched to the gun-defined longitudinal state through

$$R_{56}^{\mathrm{tot}} = R_{56}^{\mathrm{gun}} + R_{56}^{\mathrm{u}} + R_{56}^{\mathrm{DBA}} + R_{56}^{\mathrm{d}}. \tag{10}$$

When $R_{56}^{\mathrm{tot}} \approx 0$, the momentum-dependent timing modulation generated at the gun exit is compensated by the downstream transport. This condition is meaningful only because the 2.33-cell gun provides a clean momentum–TOF correlation and therefore a well-defined R_{56}^{gun}.

Figure 3 shows the cathode-to-sample timing response of the 2.33-cell gun matched to the DBA transport. Panel (a) gives the beam energy, with the white dashed contour marking 3 MeV. Panel (b) gives the relative cathode-to-sample TOF, and panels (c,d) give the TOF sensitivities to RF amplitude and phase. The vertical green line in panel (c) coincides with the 3 MeV contour in panel (a), showing that the isochronous condition is fulfilled at the updated gun energy. In panel (d), the green dashed line is the phase of minimum cathode-to-sample TOF for each RF amplitude, while the red dashed line denotes the nominal amplitude condition. Their intersection defines the updated operating point, $E_0 = 45\,\mathrm{MV/m}$ and $\phi_0 = 63°$.

The local sample-plane timing jitter is obtained from the two sensitivity maps as $\sigma_{t,s} \simeq [(\partial T_s/\partial A\,\sigma_A)^2 + (\partial T_s/\partial \phi\,\sigma_\phi)^2]^{1/2}$. Figure 4 uses $\sigma_A/A = 0.05\%$ and a phase jitter of 0.2 ps ($\simeq 0.21°$ at 2.856 GHz). Near 45 MV/m and 63°, the calculated jitter is below 1 fs; even for about 3×10^{-3} energy offset it remains within several femtoseconds.

For the GPT tracking reported here, the beam at the gun exit has a kinetic energy of 3 MeV, an rms bunch length of 100 fs, a charge of 0.1 pC, and a normalized emittance of about 10 nm · rad. Using the DBA transport parameters following Ref. [7], the beam is compressed to 940 as rms at the sample with a remaining charge of about 10 fC. Under RF-amplitude, RF-phase, charge, and magnet-field jitters of

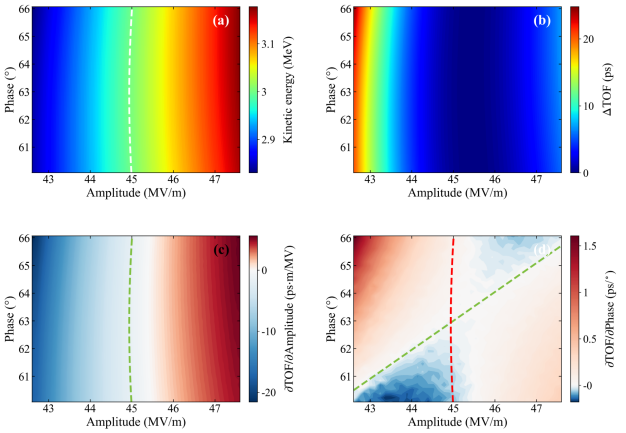

Figure 3: Cathode-to-sample timing response: (a) energy, (b) relative TOF, (c) amplitude sensitivity, and (d) phase sensitivity. The white dashed line in (a) marks 3 MeV.

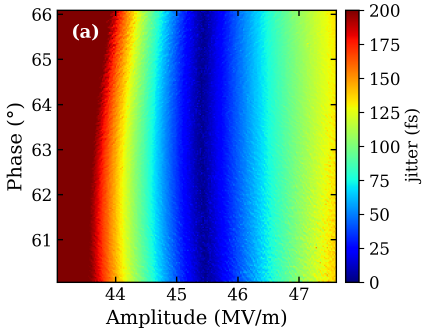

Figure 4: Calculated sample arrival-time jitter versus RF amplitude and launch phase. The nominal operating point lies in the sub-femtosecond region.

0.05%, 0.2 ps, 3%, and 0.01% rms, respectively, the sample-plane arrival-time jitter is 600 as rms. When the source jitters are scanned independently, the timing jitter is 518 as rms from RF-amplitude jitter alone and 167 as rms from RF-phase jitter alone.

The local maps show that the residual sample-plane timing noise is mainly amplitude-driven, while the phase-driven term stays secondary because the gun operates close to the common maximum-energy and minimum-TOF phase. The matched transport therefore acts on a well-defined source dispersion rather than on two decoupled RF responses.

CONCLUSION

This paper addresses attosecond MeV-UED source design by introducing a 2.33-cell RF gun with controlled longitudinal dispersion. Operating the gun near the common maximum-energy and minimum-TOF phase yields a clean gun-exit R_{56}^{g} at 3 MeV; with the matched DBA, a 100 fs source is compressed to 940 as rms with 600 as rms sample arrival-time jitter. These results support controlled gun dispersion as a practical route toward attosecond UED beamlines.

REFERENCES

[1] R. Srinivasan, V. A. Lobastov, C.-Y. Ruan, and A. H. Zewail, "Ultrafast electron diffraction (UED): A new development for the 4D determination of transient molecular structures," *Helv. Chim. Acta*, vol. 86, no. 6, pp. 1761-
doi:10.1002/hlca.200390147

[2] J. B. Hastings et al., "Ultrafast time-resolved electron diffraction with megavolt electron beams," *Appl. Phys. Lett.*, vol. 89, no. 18, p. 184109, 2006.
doi:10.1063/1.2372697

[3] Y. Cheng, Q. Gu, and C. Feng, "Multidimensional phase space manipulation for attosecond electron bunch compression," *Phys. Rev. Accel. Beams*, 2026.
doi:10.1103/3t5l-mz61

[4] H. W. Kim et al., "Towards jitter-free ultrafast electron diffraction technology," *Nat. Photonics*, vol. 14, no. 4, pp. 245–249, 2020.
doi:10.1038/s41566-019-0566-4

[5] K.-J. Kim, "RF and space-charge effects in laser-driven rf electron guns," *Nucl. Instrum. Methods Phys. Res. A*, vol. 275, no. 2, pp. 201–218, 1989.
doi:10.1016/0168-9002(89)90688-8

[6] S. B. van der Geer and M. J. de Loos, "The general particle tracer code: Design, implementation and application," Ph.D. thesis, Technische Universiteit Eindhoven, 2001.
doi:10.6100/IR542912

[7] F. Qi et al., "Breaking 50 femtosecond resolution barrier in MeV ultrafast electron diffraction with a double bend achromat compressor," *Phys. Rev. Lett.*, vol. 124, no. 13, p. 134803, 2020.
doi:10.1103/PhysRevLett.124.134803